J|A|C|S ARTICLES

Published on Web 07/08/2009

# Identifying the Local Structures Formed during Lithiation of the Conversion Material, Iron Fluoride, in a Li Ion Battery: A Solid-State NMR, X-ray Diffraction, and Pair Distribution Function Analysis Study

Naoko Yamakawa,[†,‡] Meng Jiang,[†] Baris Key,[†] and Clare P. Grey*[,†]

*Department of Chemistry, SUNY Stony Brook, Stony Brook, New York 11794-3400, and Research & Development Division, Energy Business Group, Sony Corporation, 1-1 Aza, Shimosugishita, Takakura, Hiwada-machi, Koriyama-shi, Fukushima 963-0531, Japan*

Received April 2, 2009; E-mail: cgrey@notes.cc.sunysb.edu

***Abstract:*** The structural transformations that occur when $FeF_3$ is cycled at room temperature in a Li cell were investigated using a combination of X-ray diffraction (XRD), pair distribution function (PDF) analysis, and magic-angle-spinning NMR spectroscopy. Two regions are seen on discharge. The first occurs between Li = 0 and 1.0 and involves an insertion reaction. This first region actually comprises two steps: First, a two-phase reaction between Li = 0 and 0.5 occurs, and the $Li_{0.5}FeF_3$ phase that is formed gives rise to a Li NMR resonance due to $Li^+$ ions near both $Fe^{3+}$ and $Fe^{2+}$ ions. On the basis of the PDF data, the local structure of this phase is closer to the rutile structure than the original $ReO_3$ structure. Second, a single-phase intercalation reaction occurs between Li = 0.5 and 1.0, for which the Li NMR data indicate a progressive increase in the concentration of $Fe^{2+}$ ions. In the second region, the conversion reaction, superparamagnetic, nanosized (~3 nm) Fe metal is formed, as indicated by the XRD and NMR data, along with some LiF and a third phase that is rich in Li and F. The charge process involves the formation of a series of intercalation phases with increasing Fe oxidation state, which, on the basis of the Li NMR and PDF data, have local structures that are similar to the intercalation phases seen during the first stage of the discharge process. The solid-state NMR and XRD results for the rutile phase $FeF_2$ are presented for comparison, and the data indicate that an insertion reaction also occurs, which is accompanied by the formation of LiF. This is followed by the formation of Fe nanoparticles and LiF via a conversion reaction.

## Introduction

One of the most important rechargeable energy storage technologies is the lithium ion battery (LIB). LIBs are used for a variety of mobile equipment, including cell phones, laptop computers, and power tools. They are also promising candidates for power sources in automotive applications. Although their performance has improved dramatically in recent years, there are still many issues that remain to be solved for the various applications. One of the most crucial ones is the energy density of the cathode (or, more accurately in a rechargeable system, the positive electrode) material.[1] Layered compounds based on $LiCoO_2$, with specific capacities of 120−150 mA h $g^{-1}$, are currently used in commercial LIBs. In these materials, lithium is stored between the layers, and lithium deintercalation and reintercalation occur during the charge and discharge cycles without significant structural change.[2] This type of reaction gives excellent cycling performance but yields only a limited capacity because of the structure and corresponding restricted valence changes of the transition metals. Recently, 3d-transition-metal binary compounds $M_xX_y$ (M = Co, Fe, Ni, Cu, etc.; X = F, O, S, N, etc.) have been extensively investigated as potential electrode materials for LIBs. Tarascon and co-workers demonstrated that these materials have specific capacities as high as 600−1000 mA h $g^{-1}$ along with excellent cycling reversibility.[3] Unlike the layered compounds, these materials react via a "conversion reaction" of the form

$$M_xX_y + nyLi \rightleftarrows yLi_nX + xM \quad (1)$$

In this reaction, micrometer-sized $M_xX_y$ decomposes to form a ~1−10 nm metallic particle/$Li_nX$ nanocomposite in the first reduction reaction. This is followed by repetitive redox cycles in which the sizes of the particles formed during these processes remain largely unchanged from cycle to cycle. The electrochemically driven nanosized confinement of the metal particles by the lithium salt $Li_nX$ is believed to enhance their electrochemical activity, providing better reversibility to the $Li_nX$−M nanocomposite.

Of the $M_xX_y$ materials, only the metal fluorides can be used as alternative positive electrode materials for LIBs because of the high operating voltages caused by their ionic character.[4,5]

[†] SUNY Stony Brook.
[‡] Sony Corporation.

(1) Tarascon, J. M.; Armand, M. *Nature* **2001**, *414*, 359–367.
(2) Mizushima, K.; Jones, P. C.; Wiseman, P. J.; Goodenough, J. B. *Mater. Res. Bull.* **1980**, *15*, 783–789.
(3) Poizot, P.; Laruelle, S.; Grugeon, S.; Dupont, L.; Tarascon, J. M. *Nature* **2000**, *407*, 496–499.
(4) Li, H.; Richter, G.; Maier, J. *Adv. Mater.* **2003**, *15*, 736–739.
(5) Li, H.; Balaya, P.; Maier, J. *J. Electrochem. Soc.* **2004**, *151*, A1878–A1885.

  

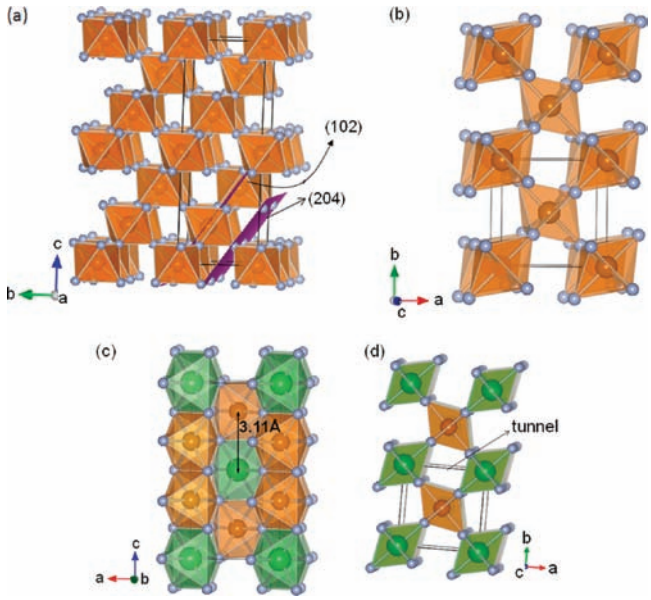


***Figure 1.*** Structures of (a) $FeF_3$, showing the $Fe^{3+}$-free (204) plane and the (102) layer containing $Fe^{3+}$ ions ($R\bar{3}C$, $ReO_3$-type structure), (b) $FeF_2$ ($P4_2/mnm$, tetragonal, rutile structure), and (c, d) $Li_{1/2}FeF_2$ ($P4_2/mnm$, tetragonal, trirutile structure) along the (c) *a* and (d) *c* directions. Blue, green, and orange spheres correspond to F, Li, and Fe, respectively.

However, fluorides are usually large-band-gap insulators, making it more difficult to develop these materials for LIBs. To overcome this difficulty, Amatucci and co-workers have proposed the use of carbon−metal−fluoride nanocomposites (CMFNCs).[6,7] The drastic reduction of $MF_y$ particle size and the highly conductive carbon matrix connecting the nanograins enhance the electrochemical activity dramatically in the first cycle and result in excellent reversibility in subsequent cycles, in part as a result of the stability of surfaces coated by carbon materials.

Iron(III) fluoride ($FeF_3$) has a theoretical capacity of ~200 mA h $g^{-1}$ in the 4.5−2.5 V region and 400 mA h $g^{-1}$ in the 2.5−1.5 V region during the conversion reaction. The electrochemical activity of this fluoride was first reported by Arai et al.[8] Subsequently, Li et al.[5] and Badway and co-workers[6,7,9] have proposed the following reaction schemes for the two regions:

$$FeF_3 + Li \rightarrow LiFeF_3 \quad (4.5-2.5\ V) \qquad (2)$$

$$LiFeF_3 + 2Li \rightarrow Fe^0 + 3LiF \quad (2.5-1.5\ V) \qquad (3)$$

In the first region (eq 2), $Li^+$ is inserted into the $FeF_3$ framework first via a two-phase reaction to form $Li_{0.5}FeF_3$ and then via a single-phase reaction to form $LiFeF_3$. This process appears to be fully reversible. $FeF_3$ adopts a rhombohedrally distorted version of the $ReO_3$ structure ($BX_3$, space group $R\bar{3}C$) (Figure 1). The structure is related to perovskite $ABX_3$ and comprises corner-sharing $FeF_{6/2}$ octahedra that are connected to form a three-dimensional tunnel structure. The $Fe^{3+}$ ions lie on the (102) planes of the rhombohedral structure, while the (204) planes contain the vacant A sites that are available for $Li^+$ insertion. $Li^+$ insertion, however, appears to result in a change in the structure of the Fe sublattice, since pronounced changes in the XRD patterns are seen upon insertion of 0.5 Li per $FeF_3$ unit.[6] One driving force for this structural rearrangement may come from the fact that the vacant A sites are actually too large for $Li^+$. In the subsequent step (eq 3), $LiFeF_3$ is reported to decompose to form LiF and Fe metal, and this part of reaction also has been found to be reversible when a carbon−$FeF_3$ nanocomposite is used.

In regard to the reconversion reaction, Badway et al.[7] have proposed that the Fe metal and LiF react to form a "$FeF_2$ rutile-like" structure (Figure 1) instead of the initial $FeF_3$ structure. Consistent with this, the electrochemistry of $FeF_2$ is quite similar to that of $FeF_3$ after the first cycle. However, the observed capacity corresponding to the extraction of three $Li^+$ cannot be explained with this mechanism scheme alone. Recently, the first-principles calculations of Doe et al.[10] suggested that a series of intermediate phases could be formed during the electrochemical process, their exact nature being controlled by the differences in the kinetics of the diffusion of the different ions or atoms in the system ($F^-$, $Fe^{n+}$, $Li^+$). Specifically, they proposed that the $ReO_3$ structure rearranges to form a series of stable phases derived from rutile upon discharge; they also suggested that the inverse spinel phase $Li_{3/2}Fe_{3/4}F_3$ may be formed during the lower-voltage process. Their calculations suggested that the defect trirutile structure, $Fe_{2/3}F_2$, (space group $P4_2/mnm$) is formed at the end of first charge. This material contains $Fe^{3+}$ ions, accounting for the capacity observed upon the first charge and in subsequent cycles. However, in view of the disorder and small particle sizes seen in this nanocomposite system, it is difficult to validate some of the hypotheses of this paper experimentally.

NMR spectroscopy is in principle a powerful technique for probing short-range ordering,[11] making it an ideal tool for understanding the mechanism of reactions involving nanosized particles. However, the materials studied here are either highly paramagnetic or ferromagnetic, making them extremely challenging (and sometimes impossible) to study by high-resolution NMR methods. However, we show here the surprising result that we can nonetheless extract considerable detail concerning the local structure, iron oxidation state, and magnetic properties with this approach, which we used to probe the details of the conversion/reconversion reaction mechanisms for $FeF_3$. The results are combined with X-ray diffraction (XRD) and pair distribution function (PDF) analysis of the XRD data, the latter representing another excellent tool for probing short-range ordering of disordered materials and nanoparticles[12] and for testing theories for structural rearrangements.[10] To achieve the superior electrochemical performance of $FeF_3$, carbon-coated nano-$FeF_3$ (CCN-$FeF_3$) was used. The results are compared with the diffraction and NMR data following lithium insertion into $FeF_2$.

## Experimental Section

**Materials Preparation.** CCN-$FeF_3$ was prepared by high-energy milling of $R\bar{3}C$ $FeF_3$ (Kojundo) with carbon black (Ketjen Black

(6) Badway, F.; Cosandey, F.; Pereira, N.; Amatucci, G. G. *J. Electrochem. Soc.* **2003**, *150*, A1318–A1327.
(7) Badway, F.; Pereira, N.; Cosandey, F.; Amatucci, G. G. *J. Electrochem. Soc.* **2003**, *150*, A1209–A1218.
(8) Arai, H.; Okada, S.; Sakurai, Y.; Yamaki, J.-i. *J. Power Sources* **1997**, *68*, 716–719.
(9) Cosandey, F.; Al-Sharab, J. F.; Badway, F.; Amatucci, G. G.; Stadelmann, P. *Microsc. Microanal.* **2007**, *13*, 87–95.
(10) Doe, R. E.; Persson, K. A.; Meng, Y. S.; Ceder, G. *Chem. Mater.* **2008**, *20*, 5274–5283.
(11) Grey, C. P.; Dupre, N. *Chem. Rev.* **2004**, *104*, 4493–4512.
(12) Breger, J.; Dupre, N.; Chupas, P. J.; Lee, P. L.; Proffen, T.; Parise, J. B.; Grey, C. P. *J. Am. Chem. Soc.* **2005**, *127*, 7529–7537.

International Company). Stoichiometric mixtures [$FeF_3$/carbon black = 80:20 (w/w)][7] were placed inside a steel milling cell with zirconia balls. Milling was performed for 3 h in a high-energy milling machine (Rotec) at 500 rpm. Carbon-coated nano-$FeF_2$ (CCN-$FeF_2$) was also prepared, using the same procedure as for CCN-$FeF_3$.

**Electrochemical Characterization.** Positive electrodes were prepared by mixing the following components in an 80:15:5 (w/w) ratio in *N*-methylpyrrolidinone: the active material (CCN-$FeF_3$ or CCN-$FeF_2$), graphite as an electronic conductor, and polyvinylidene fluoride (PVDF) as a binder. The slurry was coated on aluminum foil and dried at 100 °C until the solvent had evaporated completely. Coin-type (2032) cells were assembled in an argon-filled glovebox with Li metal foil ($^6$Li foil for $^6$Li NMR experiments) (Aldrich) as the anode, polypropylene separators (Celgard), and a 1 M solution of $LiPF_6$ in 1:1 ethylene carbonate (EC)/dimethyl carbonate (DMC) as the electrolyte. No binder was used to prepare the samples for the synchrotron XRD experiments and samples Li1.7, Li3.0, and C_Li0.5 for $^{19}$F NMR analysis. An 85:15 (w/w) mixture of active material (CCN-$FeF_3$ or CCN-$FeF_2$) and carbon black was used for the positive-electrode mixture in Swagelok-type cells with Whatman GF/D fiber as the separator. Electrochemical experiments were carried out with a battery cycler (Arbin Instruments, College Station, TX) in galvanostatic mode at a C/100 rate of 1.0−4.0 V. The samples for the NMR, XRD, and PDF studies were recovered from cycled batteries stopped at various states of charge by disassembling them inside an argon-filled glovebox and scraping the powder mixture from the current collectors. The electrodes were not washed in order to ensure that the solid electrolyte interface (SEI) is left intact and to prevent any possible loss of nanoparticles that might result from the rinsing step. The samples were either packed in sample rotors (for NMR) or capillaries (for XRD and PDF).

**X-ray Diffraction.** For the characterization of the ball-milled samples, bench-type X-ray diffraction (XRD) was performed on a Rigaku powder X-ray diffractometer equipped with a Cr-target X-ray tube (Cr K$\alpha_1$, $\lambda$ = 2.2898 Å). A range of 2$\theta$ values from 20 to 120° with a scanning rate of 1 deg/min and a step size of 0.02° was used. To analyze the structural changes during cycling, high-resolution XRD was carried out on the cycled samples at beamline 11-BM at the Advanced Photon Source (APS) at Argonne National Laboratory ($\lambda$ = 0.4001 Å)[13,14] and also at the X16C beamline at the National Synchrotron Light Source (NSLS) at Brookhaven National Laboratory ($\lambda$ = 0.6881 Å). For convenience, the values shown in this paper were converted to those corresponding to Cu K$_\alpha$ ($\lambda$ = 1.5406 Å).

**Pair Distribution Function Analysis.** PDF analysis was performed on X-ray synchrotron powder diffraction data for discharged CCN-$FeF_3$ collected at the 11-ID-XOR (11-ID-B) beamline at the APS. The data were acquired using a Ge−αSi 2D detector with an X-ray energy of 90 keV (0.134024 Å wavelength), as described previously.[12] A $CeO_2$ standard was employed to calibrate the sample-to-detector distance and the tilt of the image plate (IP) to the beam path. Data were obtained from the powder sample in transmission geometry. The IP data were integrated and converted to intensity readings versus 2$\theta$ with the Fit2D software. The PDF data were generated using the PDFgetX2 program.[15] The measured intensity was corrected for the absorption of the glass capillary by background subtraction. Corrections for multiple scattering, X-ray polarization, sample absorption, Compton scattering, and Laue diffuse scattering were then applied as described by Chupas et al.[16] to obtain the structure function $S(Q)$. A detector efficiency correction was also included. Direct Fourier transformation of the reduced structure function $F(Q) = Q[S(Q) - 1]$ up to $Q_{max}$ = 23.5 Å$^{-1}$ gave $G(r)$, the pair distribution function. Analysis and the fitting of the data were done using the PDFgui software.[17]

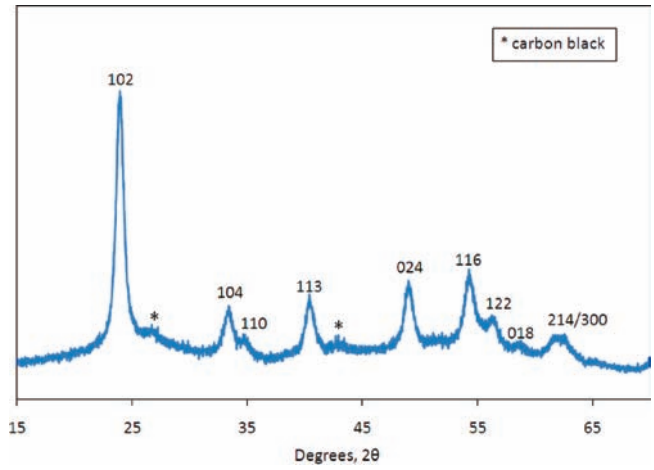


***Figure 2.*** XRD pattern of CCN-$FeF_3$ prepared by high-energy ball milling. The peaks are indexed with an $R\bar{3}C$ space group.

**MAS NMR Spectroscopy.** $^7$Li and $^6$Li magic-angle-spinning (MAS) NMR spectroscopy was performed on discharged and charged CCN-$FeF_3$ samples with a 1.8 mm probe on a CMX-200 spectrometer using a magnetic field of 4.7 T. A spinning speed of 30 kHz and a rotor-synchronized spin−echo sequence ($^\pi/_2$−$\tau$−$\pi$−$\tau$−acq) were used to acquire the spectra. The $^7$Li spectra were collected at an operating frequency of 77.10 MHz with $^\pi/_2$ pulses of 2.5 $\mu$s and a delay time of 1.0 s. The spectrum was referenced to 1 M $^7$LiCl in $H_2O$ at 0 ppm. Estimates of the $^7$Li spin−spin transverse relaxation time $T_2$ under MAS were made for selected samples using an operating frequency of 77.10 MHz and the relevant experimental conditions described above by collecting spectra as a function of spinning speed and number of rotor periods (and thus with different values of $\tau$ ranging from 31 to 264 $\mu$s) in a spin−echo experiment (see Figure S3 in the Supporting Information).

$^6$Li NMR spectra were collected at an operating frequency of 29.46 MHz with $^\pi/_2$ pulses of 3.5 $\mu$s and a delay time of 0.2 s. The spectrum was referenced to 1 M $^6$LiCl in $H_2O$ at 0 ppm.

$^{19}$F MAS NMR spectra were performed on cycled $FeF_3$ samples with a 3.2 mm probe on a CMX-360 spectrometer using a magnetic field of 8.46 T. The spectra were collected at an operating frequency of 338.73 MHz with a spinning speed 20 kHz and a rotor-synchronized spin−echo sequence; $^\pi/_2$ pulses of 5.75 and 3.5 $\mu$s (for different power-level settings) were used, with a delay time of 1.0 s. The spectrum was referenced to fluorobenzene at −113.8 ppm.[18]

## Results

**Pristine CCN-$FeF_3$ Characterization: Diffraction.** XRD was used to confirm the structure of the $FeF_3$ ball-milled with carbon black (CCN-$FeF_3$) and check the purity of the sample (Figure 2). The pattern of the ball-milled sample can be indexed with the same space group as the sample before milling, indicating that no significant structural changes and impurity phases were introduced during the milling process. However, a noticeable

(13) Lee, P. L.; Shu, D. M.; Ramanathan, M.; Preissner, C.; Wang, J.; Beno, M. A.; Von Dreele, R. B.; Ribaud, L.; Kurtz, C.; Antao, S. M.; Jiao, X.; Toby, B. H. *J. Synchrotron Radiat.* **2008**, *15*, 427–432.
(14) Wang, J.; Toby, B. H.; Lee, P. L.; Ribaud, L.; Antao, S. M.; Kurtz, C.; Ramanathan, M.; Von Dreele, R. B.; Beno, M. A. *Rev. Sci. Instrum.* **2008**, *79*, 085105.
(15) Qiu, X.; Thompson, J. W.; Billinge, S. J. L. *J. Appl. Crystallogr.* **2004**, *37*, 678.
(16) Chupas, P. J.; Qiu, X. Y.; Hanson, J. C.; Lee, P. L.; Grey, C. P.; Billinge, S. J. L. *J. Appl. Crystallogr.* **2003**, *36*, 1342–1347.
(17) Farrow, C. L.; Juhas, P.; Liu, J. W.; Bryndin, D.; Bozin, E. S.; Bloch, J.; Proffen, T.; Billinge, S. J. L. *J. Phys.: Condens. Matter* **2007**, *19*, 335219.
(18) Hinedi, Z. R.; Chang, A. C.; Borchardt, D. B. *Water Res.* **1997**, *31*, 877–883.

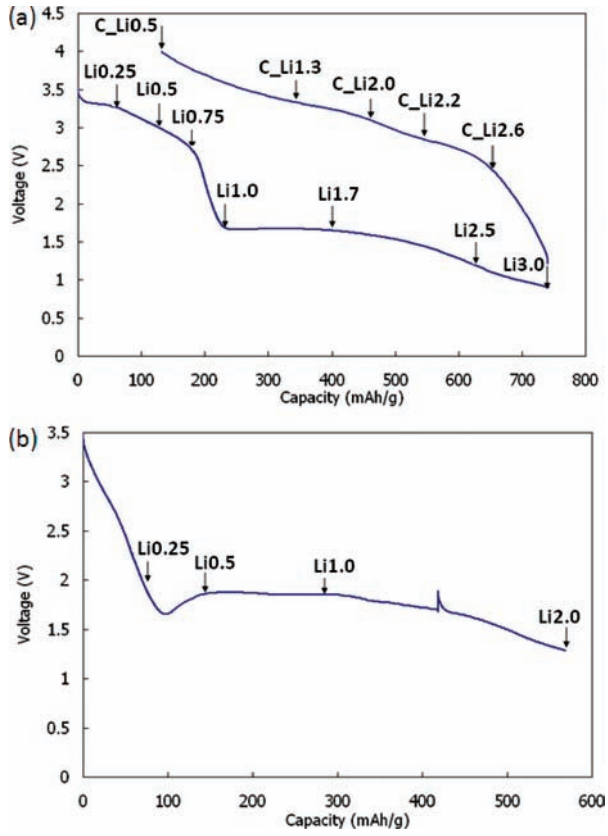


***Figure 3.*** Electrochemical curves for (a) CCN-$FeF_3$ (first cycle) and (b) CCN-$FeF_2$ (discharge only), performed at room temperature at C/100. In (b), the discharge process was interrupted at ~420 mA h $g^{-1}$, resulting in a spike; the spike maximum represents the open-circuit voltage of the cell at this state of discharge. Arrows indicate the Li content, potentials, and capacities of the different samples studied in this work.

broadening of the Bragg peaks was observed. The crystallite size determined from the Scherrer formula[19] using the (102) Bragg peak of CCN-$FeF_3$ was 8 nm, indicating that the particle size decreased considerably on ball milling.

**CCN-$FeF_3$: Electrochemical Characterization.** The electrochemical performance of CCN-$FeF_3$ was investigated in the voltage range 4.0−1.0 V (Li/$Li^+$) at room temperature at a C/100 rate (Figure 3a). A short plateau at 3.3 V was first observed, after which the voltage decreased gradually to ~2.5 V. A plateau-like region was then observed at 1.7 V, the voltage dropping slowly to 1.0 V for capacities above ~500 mA h $g^{-1}$. This behavior is similar to that found by Badway et al.,[6,7] except that their operating voltage was slightly higher, presumably because of the higher operating temperature used in their study (70 °C). The discharge reaction can be divided into two parts, as mentioned above. The first part, between 3.5 and 1.7 V, has been ascribed to an insertion reaction involving reduction of $Fe^{3+}$ to $Fe^{2+}$ (eq 1), and the second part, between 1.7 and 1.0 V, is due to the conversion reaction region involving reduction of $Fe^{2+}$ to $Fe^0$ (eq 2).[7] Our specific capacities for these two regions were 233 and 500 mA h $g^{-1}$, respectively, which are very close to the theoretical capacities of 237 and 487 mA h $g^{-1}$. The slight overcapacity in the second region is ascribed to a contribution from SEI layer formation during discharge. On charge, no obvious plateau was observed, and the voltage profile

(19) West, A. R. *Solid State Chemistry and Its Applications*; John Wiley & Sons: New York, 1992.

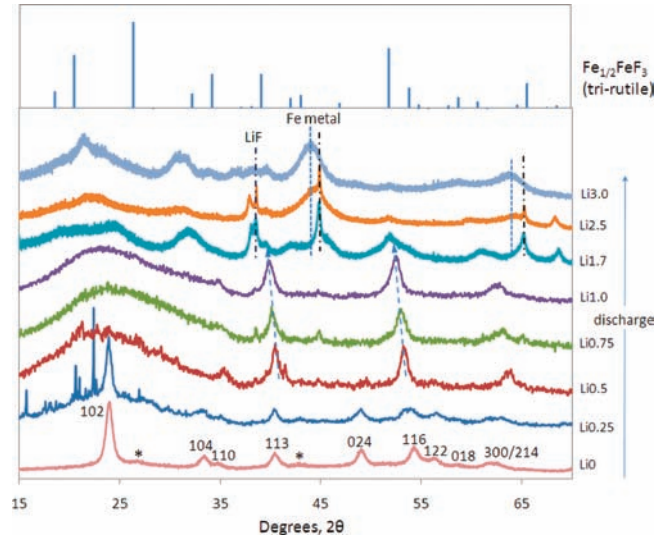


***Figure 4.*** XRD patterns of discharged $FeF_3$ samples. In this and subsequent figures, the Li content in each sample was calculated from the discharge (charge) capacity and is shown on the right-hand side. The reflections from LiF, Fe metal, and carbon are marked with black dashed lines, blue dashed lines, and asterisks, respectively. The data from the samples Li0.25, Li0.5, Li0.75, and Li1.0 were measured at the X16C beamline at the NSLS, while all of the other measurements were performed at the 11-BM beamline at the APS.

was very different from the discharge curve. A specific charge capacity of 606 mA h $g^{-1}$ was obtained, and 127 mA h $g^{-1}$ (corresponding to 0.5 Li) was not recovered. The data for $FeF_2$ in Figure 3b is provided for comparison and will be discussed later. Samples were then extracted from a series of batteries arrested at key states of discharge/charge. To aid in the interpretation of the data, these samples are labeled according to their Li content, calculated assuming 100% Coulombic efficiency. For example, Li0.25 and C_Li0.25 represent samples with a nominal stoichiometry of $Li_{0.25}FeF_3$ obtained on discharge and charge, respectively.

**High-Resolution XRD. a. Discharged CCN-$FeF_3$.** Figure 4 shows XRD patterns of discharged CCN-$FeF_3$ samples for Li = 0.25−3.0. The peak positions of the reflections of the Li0.25 sample are very similar to those of the pristine CCN-$FeF_3$ sample, except that the intensities of the reflections assigned to the $FeF_3$ phase have slightly decreased. The series of sharp peaks observed for $2\theta < 24°$ appear to be due to the decomposition of the sample, even though it was sealed in a glass capillary for the XRD measurement. The same measurement was repeated for a different sample with identical Li content but sealed in a kapton capillary. Again, a new series of additional reflections for $2\theta < 24°$ was seen. However, all of the other major reflections remained in the same position, suggesting that the reflections at lower angles are due to side reactions and decomposition of the sample that occurred after it was removed from the battery and are not inherent in the original electrochemical reaction. This Li-content sample appears to be noticeably more reactive than that at any other composition. A distinct change in the XRD pattern for the Li0.5 sample can be seen. The most intense peak for the CCN-$FeF_3$ phase, at $2\theta = 24°$, is no longer visible, and two reflections at 40 and 53° [the same positions as the (113) and (116) peaks of the CCN-$FeF_3$ phase] have grown in intensity. The loss of the 24° reflection is accompanied by a significant increase in the "amorphous" component (i.e., a broad component) in this $2\theta$ range. Two new broad reflections at $2\theta = 35$ and 63° appear, suggesting the

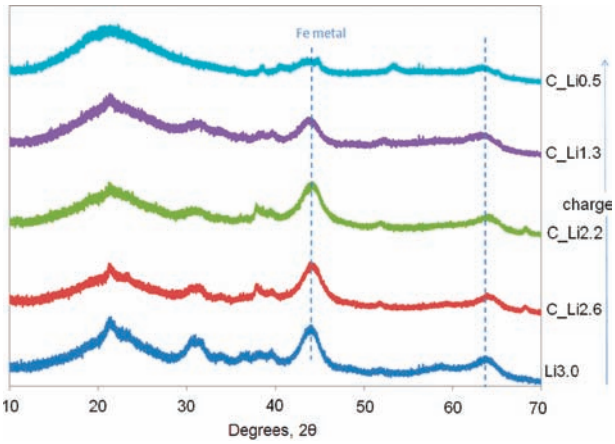


***Figure 5.*** XRD patterns of charged $FeF_3$ samples. The reflections from α-Fe are labeled with blue dashed lines. All of the data were collected at the 11-BM beamline at the APS.

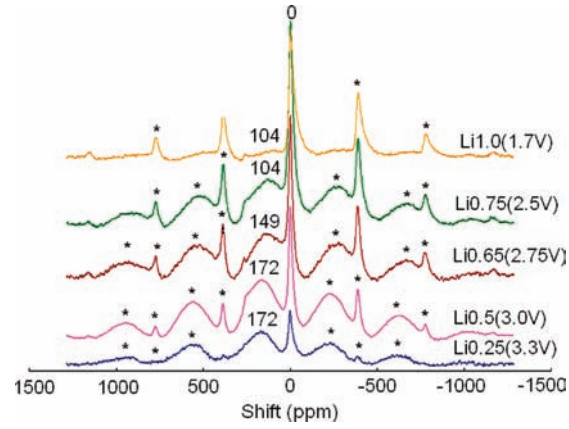


***Figure 6.*** $^7$Li MAS NMR spectra of discharged CCN-$FeF_3$ samples with Li = 0.25−1.0. The numbers in parentheses are cutoff voltages. The isotropic resonances and spinning sidebands are marked with their shifts and asterisks, respectively, in this and subsequent figures.

presence of a new phase. The disappearance of the reflections due to the CCN-$FeF_3$ phase and the appearance of a new phase ($Li_xFeF_3$) at Li = 0.5 is consistent with the plateau-like region at 3.3 V observed in the electrochemical profile, which also suggests that a two-phase reaction occurs. The reflections observed in the Li0.5 sample remain until Li = 1.0, with the peak positions shifting gradually to lower $2\theta$ values. This is consistent with the presence of a solid-solution reaction in this range, with the cell parameters of the new phase increasing on Li insertion, as expected as more $Fe^{3+}$ is reduced to $Fe^{2+}$. In previous work, the new $Li_xFeF_3$ phase was assumed to be related to the original $FeF_3$ phase, largely on the basis of the presence of reflections near 40 and 63° in both phases.[7] On the basis of this study, it appears that the positions of the two sets of reflections are coincidentally similar, but this may indicate that some structural motifs are common to the two phases. We have not been able to index the pattern on the new phase satisfactorily, largely because of the considerable breadth of the reflections.

For Li > 1.0, a gradual decrease in intensity of the reflections from the new $Li_xFeF_3$ phase is observed. However, very weak peaks at $2\theta$ = 37.5, 39.5, and 51° appear to remain from this insertion phase, indicating that there is still a small amount of this phase left at the end of discharge. The reflections from LiF and α-Fe start to appear in the XRD patterns, and those from Fe grow steadily with Li content above Li1.7. The size of the Fe particles, as determined from the Scherrer formula using the (102) Bragg peak in sample Li3.0, is only ∼3−4 nm. Surprisingly, sharp LiF reflections are seen for Li = 1.7 and 2.5, while the reflections are much broader and much less distinct for Li = 3.0, suggesting that if LiF is present in this phase, it is associated with very small particle sizes or considerable disorder. There are also some very weak reflections from LiF at Li = 0.75 and 1.0. In addition to those from LiF, Fe metal, and the $Li_xFeF_3$ phase, several broad peaks can be seen. The strongest of these reflections are located at $2\theta$ = 21 and 31° and appear to be from a new phase that most likely contains $Fe^{2+}$ in addition to $Li^+$ and $F^-$. This suggests that the process at lower voltages is much more complicated than implied by eq 2.

**b. Charged CCN-$FeF_3$.** The XRD patterns observed on charge are displayed in Figure 5. The reflections from the Fe metal become weaker with increasing state of charge, indicating that the conversion reaction is reversible. Weak LiF reflections are still seen in the C_Li0.5 sample. The reflections at $2\theta \approx 21$ and 31° stay in the same position in all of the charged samples but decrease gradually in intensity and disappear at the end of charge. Another set of weaker peaks, including those at $2\theta$ = 37.5, 39.5, and 51° ascribed to the $Li_xFeF_3$ phase as discussed above, are visible until the end of charge, but the significant shifts observed for these reflections in going from the fully discharged sample to the C_Li0.5 sample make any further analysis extremely difficult. All of the reflections for the charged samples are generally broad and weak, and no highly crystalline phases are observed in any of the samples. Nanosized particles/composites are clearly formed on charge, at least for reactions performed at room temperature.

**$^{6,7}$Li MAS NMR Spectroscopy. a. Discharged CCN-$FeF_3$.** Two major resonances in the $^7$Li MAS NMR spectra of discharged CCN-$FeF_3$ samples with Li = 0.25−1.0 can be seen (Figure 6), one at ∼0 ppm and the other between 104 and 172 ppm. The small shift of the 0 ppm resonance indicates that it is due to diamagnetic materials (e.g., $Li_2O$, LiF, etc.) present in the SEI layer or salts in the electrolyte. The increase in this resonance is due to SEI layer formation during the discharge process and possibly the formation of some LiF. On the basis of our previous work, the large shift seen for the second resonance is ascribed to the transferred hyperfine (Fermi contact) interaction between the lithium nuclear spins and the unpaired electrons of the transition-metal ions, which occurs via transfer through Li−F−$Fe^{2+/3+}$ bonds.[11] The observation of the shifted resonance provides clear evidence that lithium is inserted into an iron fluoride structure and that the lithium is in close proximity to the Fe ions ($Fe^{2+}$ and $Fe^{3+}$). The broadening of the resonance is ascribed to the presence of a range of Li local environments and the short spin−lattice ($T_1$) and spin−spin ($T_2$) relaxation times of the $^7$Li nuclei; the through-space and through-bond interactions of the Li nuclei with the fluctuating electronic moments associated with the $Fe^{2+}$/$Fe^{3+}$ ions provide an effective relaxation mechanism. On the basis of our earlier studies of a series of $LiFeO_2$ polymorphs, whose $^6$Li spectra contained resonances at frequencies in the 280−520 ppm range,[20,21] we ascribe the smaller shift of 172 ppm seen in this system to (*i*) the presence of both $Fe^{2+}$ and $Fe^{3+}$ ions in the local coordination

(20) Kim, J.; Nielsen, U. G.; Grey, C. P. *J. Am. Chem. Soc.* **2008**, *130*, 1285–1295.
(21) Nielsen, U. G.; Paik, Y.; Julmis, K.; Schoonen, M. A. A.; Reeder, R. J.; Grey, C. P. *J. Phys. Chem. B* **2005**, *109*, 18310–18315.

environment of Li and (*ii*) the decreased covalence of the Fe−F bonds relative to Fe−O bonds. $Fe^{2+}$ ions in general result in smaller hyperfine shifts than $Fe^{3+}$ ions, due in part to (a) the smaller number of unpaired electrons and (b) the decreased covalence of $Fe^{2+}$−X versus $Fe^{3+}$−X (X = $O^{2-}$, $F^-$) bonds, resulting in less effective transfer of spin density from the $Fe^{2+}$ d orbitals to the s orbitals of Li. For example, larger positive $^{6,7}$Li hyperfine shifts are seen for local environments containing $Fe^{3+}$ as opposed to $Fe^{2+}$ ions in disordered/cycled olivine ($LiFePO_4$) and Nasicon [$Li_3Fe_2(PO_4)_3$] materials.[22,23] Smaller transferred hyperfine shifts are expected for fluorides vs oxides, since the increased ionic character of the bonds should most likely result in less effective transfer of spin density, but shift calculations or experimental data from relevant model compounds are required to confirm this hypothesis. The peak position remains constant at 172 ppm for both the Li0.25 and Li0.5 samples, and its intensity gradually increases with Li content; the constant shift indicates that the average oxidation state of the Fe ions in local environments surrounding Li remains unchanged. This is consistent with the two-phase region proposed on the basis of the electrochemical results, involving a "Li-free" phase, CCN-$FeF_3$, and a second phase, $Li_yFeF_3$ ($y \approx 0.5$). A gradual shift of the 172 ppm resonance to lower frequency is observed in going from Li = 0.5 to 0.75, in agreement with a solid-solution reaction that involves insertion of Li into the $Li_{0.5}FeF_3$ structure with concomitant reduction of $Fe^{3+}$ to $Fe^{2+}$. However, the intensity of the $^7$Li resonance does not increase with further Li insertion but instead broadens noticeably and almost disappears into the baseline in the spectrum for the Li1.0 sample. The broadening is ascribed in part to the short $T_2$ relaxation time of this sample, which appears to be related to the presence of high-spin $Fe^{2+}$ ions. $T_2$ values were estimated under MAS for the samples and gave values of ~0.24 ms for the 172 ppm resonance in the Li0.5 sample and ~0.17 ms for the peak at 104 ppm in the Li1.0 sample (see Figure S3 in the Supporting Information). These short $T_2$ relaxation times result in some loss of signal intensity, particularly for the Li1.0 sample, in the spin−echo experiment used to acquire the spectra (where $2\tau = 67$ $\mu$s, resulting in ~30% loss of signal); the relaxation data are, however, indicative of a distribution of $T_2$ times (Figure S3), and it is possible that we failed to detect components of the signal with faster relaxation times. An extremely weak resonance is also seen at 260 ppm for Li ≥ 0.5. Although the shift of this resonance is close to that of metallic Li, we tentatively ascribe this resonance to an impurity such as $Li_xFeO_2$. Some evidence for fluorination of the carbon during ball-milling has been seen in analogous $CuF_2$−carbon nanocomposites, and it is possible that these phases could be lithiated at these potentials, possibly giving rise to this resonance.[24]

$^6$Li NMR was performed on the same discharged Li = 0.5−1.0 samples to ensure that all of the lithium signals were observed. $^6$Li ($I = 1$) has smaller quadrupolar and gyromagnetic moments than $^7$Li, which generally results in noticeably longer $T_1$ times and, for paramagnetic materials, higher-resolution spectra with fewer spinning sidebands, making their interpretation easier.[11] The $^6$Li spectra (Figure 7) are consistent with the $^7$Li NMR results: two resonances are observed in the spectra, one at 0 ppm and the other between 104 and 172 ppm. The spectrum of the Li1.0 sample now clearly shows the presence of the 104 ppm resonance, also confirming that no significant shift in this resonance is seen between Li = 0.75 and 1.0.

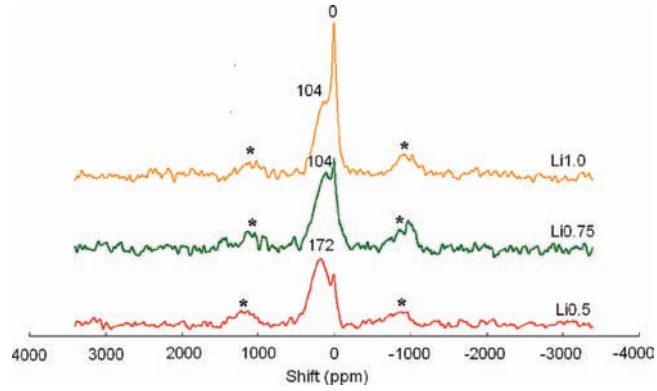


***Figure 7.*** $^6$Li MAS NMR spectra of discharged CCN-$FeF_3$ samples with Li = 0.5−1.0.

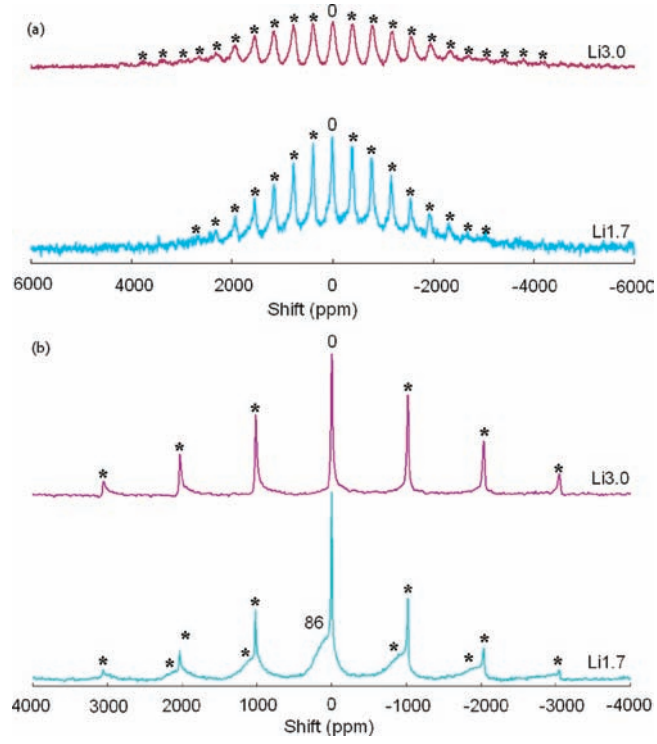


***Figure 8.*** (a) $^7$Li and (b) $^6$Li NMR spectra of discharged CCN-$FeF_3$ samples with Li = 1.7 and 3.0.

The $^7$Li NMR spectra of discharged CCN-$FeF_3$ samples in the second region, with Li = 1.0−3.0 (Figure 8a) are noticeably different from those in the first region. Only the resonance at 0 ppm can be clearly seen, along with sidebands that spread over more than 5000 ppm. The width of the sideband envelope and the broadening of the individual peaks within the sideband manifold both increase significantly at deeper discharge, consistent with the formation of iron nanoparticles. In general, the ferromagnetic properties of iron should cause significant problems for the NMR experiment, especially while spinning the sample and tuning the NMR probe. However, no problems were encountered, and spectra were obtained under the same experi-

(22) Kim, J.; Middlemiss, D.; Zhou, B.; Masquelier, C.; Grey, C. P. In preparation.
(23) Hamelet, S.; Gibot, P.; Casas-Cabanas, M.; Bonnin, D.; Grey, C. P.; Cabana, J.; Leriche, J.-B.; Rodriguez-Carvajal, J.; Courty, M.; Levasseur, S.; Carlach, P.; van Thournout, M.; Tarascon, J.-M.; Masquelier, C. *J. Mater. Chem.* **2009**, in press.
(24) Badway, F.; Mansour, A. N.; Pereira, N.; Al-Sharab, J. F.; Cosandey, F.; Plitz, I.; Amatucci, G. G. *Chem. Mater.* **2007**, *19*, 4129–4141.

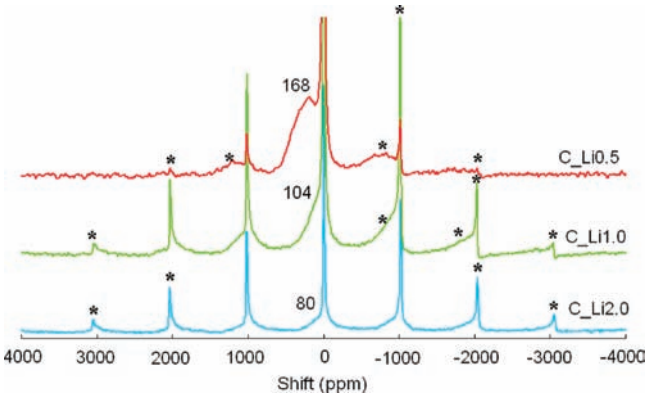


***Figure 9.*** $^{6}$Li MAS NMR spectra of charged CCN-$FeF_3$ samples with Li = 0.5−2.0.

mental conditions as used for the other samples with lower lithium content. This indicates that the iron metal is not ferromagnetic and that superparamagnetic particles are formed. This is in agreement with the diffraction data, which suggested that the Fe particle size was ∼3−4 nm; particle sizes of 6.6 nm and below exhibit superparamagnetic properties.[25] The large sideband manifolds are ascribed to the through-space dipolar electron−nuclear interactions between the Li nuclei in the diamagnetic phases and the local magnetic fields caused by the superparamagnetic particles in the static field inside the NMR magnet.

The $^{6}$Li NMR spectra of the same samples (Figure 8b) similarly contain broad sideband envelopes, but because of the smaller gyromagnetic ratio ($\gamma$) of $^{6}$Li,[11] both the individual peaks within the sideband manifold and the overall width of the manifold (in Hz) are narrower than those seen in the $^{7}$Li NMR spectra. The electron−nuclear dipolar coupling interaction scales linearly with the static magnetic field and gyromagnetic ratio and thus is smaller for $^{6}$Li than for $^{7}$Li, in units of Hz, and more readily removed by MAS. A resonance at 86 ppm can now be clearly observed in the Li1.7 sample. This resonance is assigned to a lithium environment in an insertion phase, with a higher $Fe^{2+}/Fe^{3+}$ ratio. The intensity of this resonance is much weaker than that of the 104 ppm resonance in the $^{6}$Li spectrum of the Li1.0 sample, presumably because of the onset of the conversion reaction.

**b. Charged CCN-$FeF_3$.** The $^{6}$Li NMR spectra of the charged CCN-$FeF_3$ samples for Li = 0.5−3.0 (Figure 9) resemble those seen on discharge and consist of two sets of isotropic resonances, one at 0 ppm and the other between 80 and 168 ppm. The width of the spinning-sideband manifold of the 0 ppm resonance decreases while the intensity of the resonance between 80 and 168 ppm increases and gradually shifts in frequency on going from sample C_Li2.0 to C_Li0.5. The former indicates that the concentration of superparamagnetic iron nanoparticles decreases on charge. The presence of the shifted resonances at hyperfine shift positions very similar to those seen on discharge suggests that the same lithium insertion environments return almost immediately on charge. Furthermore, the fact that the shift of the resonance in the C_Li0.5 spectrum (168 ppm) is close to that for the Li0.5 sample obtained on discharge (172 ppm) indicates that $Fe^{2+}$ and $Fe^{3+}$ coexist at the end of charge and that the average iron valence state in the two compounds is similar (i.e., close to $Fe^{2.5+}$).

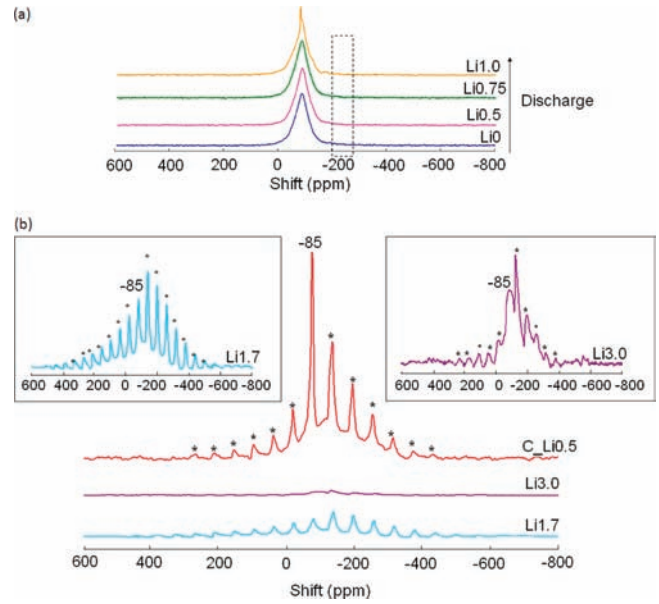


***Figure 10.*** $^{19}$F MAS NMR spectra of (a) discharged CCN-$FeF_3$ samples with Li = 0−1.0 and (b) discharged samples with Li = 1.7 and 3.0 and a charged CCN-$FeF_3$ sample with Li = 0.5. Only the spectra of the samples shown in (a) contain PVDF as a binder. The insets correspond to enlargements of the spectra of CCN-$FeF_3$ with Li = 1.7−3.0 between −600 and 800 ppm. The dashed rectangle indicates the expected location of the isotropic LiF resonance.

**$^{19}$F MAS NMR.** Since the $^{6,7}$Li signal of LiF overlaps with the signals from the diamagnetic components from the electrolyte and SEI layers, $^{19}$F ($I = {}^{1}/_{2}$, 100% natural abundance) NMR spectroscopy was performed on both the discharged and charged CCN-$FeF_3$ samples to monitor the formation of this phase. Figure 10a shows the $^{19}$F NMR spectra of the discharged CCN-$FeF_3$ samples in the first region, with Li = 0.5−1.0. The $^{19}$F NMR signal in $FeF_3$ is not readily observed because $F^-$ is directly bound to the $Fe^{3+}$ paramagnetic ions. A broad component centered around −100 ppm can be seen and is due to the fluorine background in the probe and the PVDF binder. Other than this signal, no isotropic resonances are observed until Li > 0.75, where a peak at −85 ppm is seen in Li1.0 sample. This peak is ascribed to fluorine components such as $LiP_xO_yF_z$ in the SEI layer. These compounds are formed when EC/DMC/$LiPF_6$ is used as the electrolyte[26] and represent hydrolysis products of $PF_6^-$ due to water present in the system. They may also be formed as a result of the decomposition of the electrolyte, which generates protons; this is most likely the case here, since the resonance is not seen until Li = 1.0. No resonance due to LiF (which resonates at −200 ppm[27]) is observed in these spectra, indicating that this species is not formed in significant concentrations in these samples, consistent with the ex situ XRD results (Figure 4).

The discharged CCN-$FeF_3$ samples with Li > 1.0 and the charged CCN-$FeF_3$ sample C_Li0.5 (Figure 10b) do not contain PVDF, consistent with the decrease in intensity of the broad signal at −100 ppm. In the spectrum of the discharged sample Li1.7, significant peak broadening similar to that observed in the $^{6,7}$Li NMR spectra is seen, consistent with the formation of superparamagnetic iron nanoparticles. Again, only one resonance

(25) Liao, P.; MacDonald, B. L.; Dunlap, R. A.; Dahn, J. R. *Chem. Mater.* **2008**, *20*, 454–461.
(26) Plakhotnyk, A. V.; Ernst, L.; Schmutzler, R. *J. Fluorine Chem.* **2005**, *126*, 27–31.
(27) Meyer, B. M.; Leifer, N.; Sakamoto, S.; Greenbaum, S. G.; Grey, C. P. *Electrochem. Solid-State Lett.* **2005**, *8*, A145–A148.

at −85 ppm due to the SEI is clearly resolved. Spectra were acquired at different spinning speeds to confirm that nothing is hidden under the spinning sideband at −200 ppm in Figure 10b, but these experiments did not reveal any evidence for LiF, although this should be observed in this voltage range. This indicates either that LiF is not present or that it is so intimately surrounded by Fe nanoparticles that the dipolar interactions with these particles are sufficiently large to wash out the LiF signal. Some of the LiF may also be doped with $Fe^{2+}$. The effect of the Fe particles on the $^{19}F$ NMR spectra is much more severe than on the $^{6,7}Li$ spectra, because of the higher $\gamma$ value for $^{19}F$ and the higher magnetic field used to acquire the spectra, and only a very weak $^{19}F$ signal is seen for the Li3.0 sample. The return of the −85 ppm resonance in the spectrum of the charged CCN-$FeF_3$ sample C_Li0.5 confirms that the SEI layer does not disappear in the Li3.0 sample but rather its signal must be washed out by the dipolar interactions with the Fe nanoparticles, indicating that the SEI and Fe nanoparticles must be in close proximity.

**PDF Analysis of the Conversion Reaction.** PDF analysis of the Li = 0.25 XRD data results in a pattern that is similar to the simulated pattern of $FeF_3$ (Figure 11a). A refinement of this phase was performed (Figure 11b), and the fit to the data, particularly at longer distances (10−20 Å) was reasonably good ($R_{wp}$ = 0.3404). The cell parameters extracted from this refinement are close to those of the starting phase ($a$ = 5.198 Å and $c$ = 13.34 Å for $FeF_3$[28] and $a$ = 5.095 Å and $c$ = 13.51 Å for $FeF_3$ in the Li0.25 sample). The first weak peak that is not well-captured by the refinement is due to C−C bonds (1.45 Å). The other differences between the experimental and calculated profiles are ascribed to defects in the ball-milled $FeF_3$ sample and overlap of the $FeF_3$ peaks with peaks from the new phase that on the basis of the NMR data has already started to form at this point. (It should be noted that impurity peaks are seen in the XRD pattern for this phase.) The experimental PDF patterns are very similar for Li = 0.5−1.0 but noticeably different from that of the Li0.25 sample, consistent with the XRD results. The peak positions move to higher values in this range as the structure expands and $Fe^{3+}$ is reduced to $Fe^{2+}$. This is most clearly seen for the first intense peak due to Fe−F correlations, which broadens and shifts from 1.9 to 2.05 Å on going from Li = 0.25 to 1.0. Interestingly, the pattern for the Li0.5 sample is similar to the simulated pattern for trirutile $Li_{1/2}FeF_3$, whose possible formation was suggested by Doe et al.[10] on the basis of their first-principles calculations. For example, a peak is observed at 3.11 Å that is characteristic of the short Fe−Fe (or Li−Fe) distances found in edge-sharing $FeF_6$ (or $LiF_6$ and $FeF_6$), which are present, for example, along the $c$ direction of the rutile (or trirutile) structure (as marked in Figure 1c). A broader peak is also seen at ∼4.8 Å, which corresponds to the cell dimension in the [100] direction of the rutile structure. The results suggest that at least locally, a rutile-like structure is present in this range. A refinement of the structure of the Li0.5 sample was performed with both the trirutile (TR) and $FeF_3$ structures. A slightly better refinement was obtained with the TR model ($R_{wp}$ = 0.4975 and 0.5311 for the refinements with the TR and $FeF_3$ models, respectively), as it captures more of the details of the local structure. Values of 4.75 and 9.28 (TR) and 4.99 and 14.37 Å ($FeF_3$) for the $a$ and $c$ cell parameters, respectively, were obtained. The values for the TR model are close to those obtained from the starting model ($a$ = 4.756, $c$ = 9.339 Å[10]), whereas the $c$ parameter increased noticeably in the refinement with the $FeF_3$ model (from 13.51 to 14.37 Å), consistent with the expansion of the lattice that should accompany the reduction of $Fe^{3+}$ to $Fe^{2+}$. However, the fit (with either structures) became increasingly poor for longer correlations (particularly above 8 Å), indicating that we did not capture the long-range structure of this phase (see Figure S1 in the

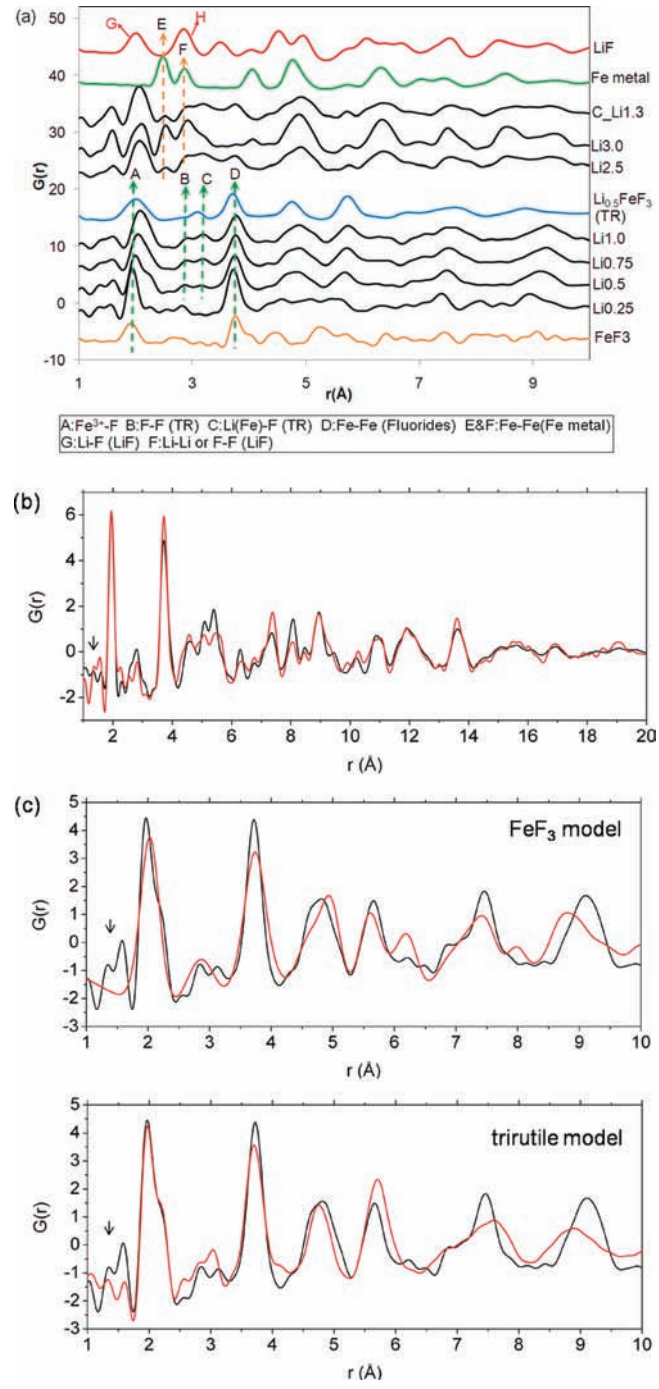


***Figure 11.*** (a) PDF patterns of the cycled CCN-$FeF_3$ samples. These are compared with the simulated patterns for $FeF_3$, $Li_{0.5}FeF_3$ (TR), LiF, and α-Fe. Characteristic correlations are labeled. (b) Refinement for the Li0.25 sample, using $FeF_3$ as a structural model. Cell parameter values of $a$ = 5.095 Å and $c$ = 13.51 Å were obtained. (c) Comparison of the refinements obtained for the Li0.5 sample using the $FeF_3$ and TR structures as structural models. In (b) and (c), red = calculated pattern, black = experimental data. The arrows indicate the closest C−C correlations.

(28) Leblanc, M.; Pannetier, J.; Ferey, G.; Depape, R. *Rev. Chim. Miner.* **1985**, *22*, 107–114.

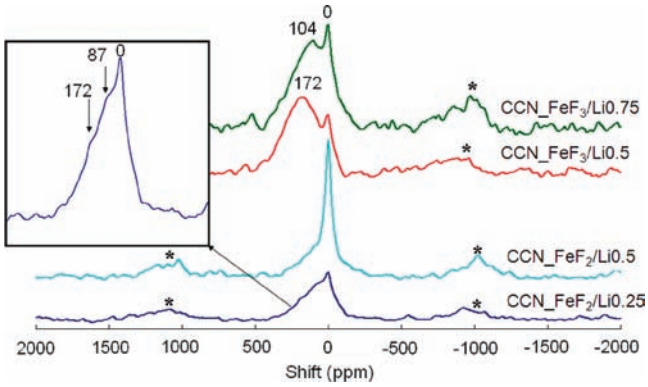


***Figure 12.*** $^{6}$Li MAS NMR spectra of discharged CCN-$FeF_2$ samples with Li = 0.25 (dark-blue) and 0.5 (cyan), compared with discharged CCN-$FeF_3$ samples with Li = 0.5 (red) and 0.75 (green). The inset shows an enlargement of the spectrum of CCN-$FeF_2$ with Li = 0.25 between 500 and −500 ppm.

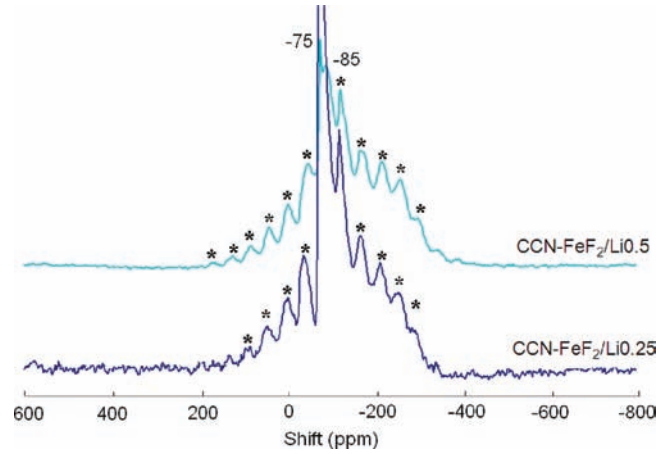


***Figure 13.*** $^{19}$F NMR spectra of discharged CCN-$FeF_2$ samples with Li = 0.25 and 0.5. The most intense resonance of the Li0.25 sample has been truncated, allowing the intensity in the region near −200 ppm to be seen.

Supporting Information for more details on these refinements and the PDF plots from 1 to 20 Å). This is consistent with the XRD results, which could not be indexed with either the trirutile or $ReO_3$ structures. We attempted to improve the fit to the data by allowing Li/Fe disorder in the trirutile structure and increasing the Fe substitution on the Li site, but no improvement was obtained. Clearly, a more detailed analysis of this data (e.g., via reverse Monte Carlo simulations[12,29]) is required to extract further information concerning both the local and long-range structure. Refinements were also performed for the Li0.75 and Li1.0 samples, and the *a* and *c* parameters obtained from these refinements increased steadily (see Figure S2 in the Supporting Information). Again, the data was better fit by the TR model, but poor fits were obtained for correlations greater than 8 Å. Noticeable deviations were seen even at 6−8 Å, suggesting that although we have captured some of the details of the local structure, we did not determine the nature of the long-range ordering.

A series of new peaks can be seen in the pattern of the Li2.5 sample (e.g., at 2.5 and 2.9 Å) in Figure 11a; these correspond to Fe−Fe distances in α-Fe. This provides more evidence that a conversion reaction takes place after Li = 1.0. The α-Fe Fe−Fe correlations become more obvious in the pattern of the Li3.0 sample, as expected. The almost complete loss in this sample of the peak at 3.8 Å, which is assigned to the Fe−Fe distances in rutile or $ReO_3$-derived structures, indicates that these phases have almost completely reacted. A broad correlation at ∼2.0 Å is still visible, which we assign to a combination of Li−F correlations from LiF (2.0 Å), Fe−F correlations due to the residual iron fluorides that remain even at deep discharge, and possibly to correlations involving the carbon. The pattern of the charged sample C_Li1.3 is very close to that of the discharged Li2.5 sample, providing strong evidence that the local structures of the two phases are very similar and thus both likely related to rutile.

**Study of the Model Compound $FeF_2$.** In order to help determine the role of the rutile structure in the $FeF_3$ conversion reactions, discharged CCN-$FeF_2$ was investigated by $^{6}$Li and $^{19}$F NMR and XRD. Two isotropic resonances can be seen in the $^{6}$Li spectra of the discharged CCN-$FeF_2$ samples Li0.25 and Li0.5 (Figure 12), a sharp one at 0 ppm and a broader one with weaker features at 87 and 172 ppm, although given the resolution and signal-to-noise ratio of these spectra, it is difficult to be sure that the latter two peaks really correspond to distinct resonances. The peak at 0 ppm is ascribed to LiF and the SEI layer, as described earlier. The resonance(s) at 87−172 ppm provide clear evidence for the interaction between the lithium spins and the unpaired electrons of iron ions, indicating that the lithium ions were inserted into the rutile (iron fluoride) lattice. The concentration of these environments decreases in going from Li = 0.25 to 0.5, presumably as more Fe metal is formed. Significantly, the shifts of these resonances are similar to those of the discharged CCN-$FeF_3$ samples Li0.5 and Li0.75, which are also shown in Figure 12 for comparison.

Two isotropic resonances are observed in the $^{19}$F NMR spectra of the discharged CCN-$FeF_2$ samples (Figure 13). The peak at −75 ppm is assigned to $LiPF_6$ from the electrolyte,[27] and the peak at −85 ppm is from the SEI layer, as discussed earlier. The peak at −200 ppm is a spinning sideband and not from LiF. This was confirmed by acquiring a spectrum with a different spinning speed. However, there does appear to be a broader component underneath the sideband manifolds that is centered at approximately −200 ppm. Sharp reflections from LiF are seen in the XRD pattern for the Li0.25 sample, as shown in Figure 14. As before, we ascribe the lack of a distinct LiF resonance either to $Fe^{2+}$ doping in LiF, strong interactions between LiF and the Fe nanoparticles, and/or the relatively low concentration of this environment. Reflections from α-Fe are not very obvious in the XRD pattern of this sample, most likely because of the small particle sizes and their low concentrations. A significant shift of all of the $FeF_2$ reflections to smaller angles is seen in going from Li = 0 to 0.25, which is seen most clearly for the 031 reflection.

The NMR and XRD results indicate that the conversion reaction happens during the early stages of discharge for CCN-$FeF_2$ but that the mechanism also involves the creation of a lithiated iron fluoride with slightly larger cell parameters. Unlike the $FeF_3$ series, no extra peaks are observed in any of the discharged samples except for the ones from LiF and Fe, indicating that the insertion phase adopts the same space group as that of pristine CCN-$FeF_2$. The reflections from $FeF_2$ then decrease steadily in intensity upon lithiation and shift slightly to lower angles, particularly from Li = 0 to 0.25. As in the

(29) Breger, J.; Kang, K.; Cabana, J.; Ceder, G.; Grey, C. P. *J. Mater. Chem.* **2007**, *17*, 3167–3174.

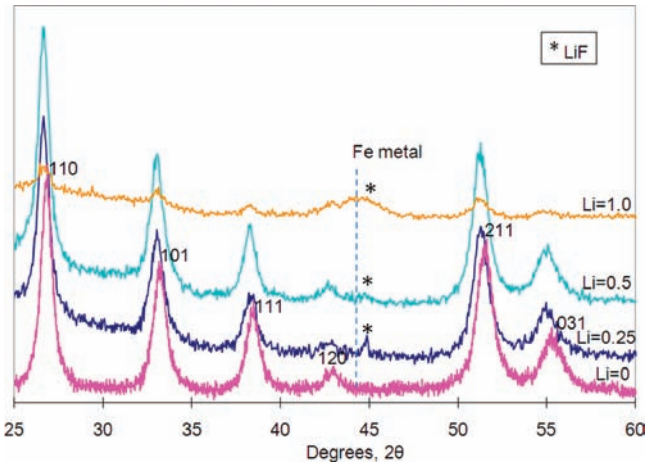


***Figure 14.*** Ex situ XRD patterns of discharged CCN-$FeF_2$ samples with Li = 0−1.0. The Li content is labeled. Pristine CCN-$FeF_2$ is indexed with the $P4_2/mnm$ space group. Reflections from LiF are labeled with asterisks, and the blue dashed line indicates the position of an Fe metal reflection.

case of $FeF_3$, a sharper LiF reflection is first observed, and it broadens noticeably on deeper discharge.

## Discussion

**Discharge Reaction Mechanism.** The first region of the discharge mechanism of $FeF_3$ (Li = 0 to ~1.0) occurs first via a first-order process (a two-phase region), as indicated by the observation of a $^{6,7}$Li resonance at 172 ppm whose frequency remains constant on going from Li = 0.25 to 0.5 and a phase transition from the $ReO_3$ structure to a new phase, $Li_yFeF_3$, ($y \approx 0.5$), as observed by XRD. From Li = 0.5 to 1.0, the Li resonance shifts gradually to lower frequency, and the reflections of the new phase shift to lower $2\theta$ values, indicating that a solid-solution reaction involving reduction of $Fe^{3+}$ is taking place in this regime. This mechanism is in qualitative agreement with the electrochemical results, where a plateau-like region exists at 3.3 V (up to Li ≈ 0.25), with the voltage dropping steadily thereafter until a Li content of 0.75. The experimentally observed decrease in voltage between Li = 0.25 and 0.5 suggests that there is a competition between the conversion of $FeF_3$ to the new $Li_{0.5}FeF_3$ phase and the insertion (or reaction) of further Li into the already formed $Li_{0.5}FeF_3$ phase in this region, since the latter process may be more kinetically favorable for experiments performed galvanostatically. The XRD and NMR experiments were performed on samples that were allowed to rest before the battery was opened, and thus, these experiments probed samples that were closer to thermodynamic equilibrium (or at least a thermodynamic local minimum). Notably, the GITT experiments of Badway et al.[7] demonstrated that the first plateau extends to Li ≈ 0.4.

The PDF patterns of the new $Li_yFeF_3$ ($0.5 \le y \le 1$) phase contain short M−M correlations (at 3.1 Å) that are ascribable to edge-sharing $FeF_6$ octahedra (or $LiF_6$ and $FeF_6$ octahedra), suggesting that at least locally, this new phase contains some of the structural features that are found in the (tri)rutile structure. The similarity of the $^{6,7}$Li NMR spectra seen in this regime with the spectra of the discharged $FeF_2$ samples is in agreement with this. A transformation from a $ReO_3$ to a rutile structure involves considerable structural reconstruction, and this may explain why the long-range structure of rutile is not seen on discharge. However, shearing transformations of $ReO_3$-type phases on reduction, leading to edge sharing of the $BX_3$ octahedra, are well-established, and this may represent a possible mechanism for the formation of some of the structural features found in rutile. A mechanism of this sort might explain the loss in the intensity of the 102 reflection from the $ReO_3$ structure in the XRD patterns upon lithiation, which was accompanied by the noticeable increase of intensity of a broader "amorphous" component at a similar range of $2\theta$ values. These types of shearing transformations occur in order to remove anion vacancies, which in this system could be formed as the first stage of fluoride ion extrusion and LiF formation:

$$Li_yFeF_3 \rightarrow Li_{y-\delta}FeF_{3-\delta} + \delta LiF \quad (4)$$

Clearly, further structural studies are required in order to solve the long-range structure of this material and determine how the structural transformations occur.

Doe et al.[10] suggested that $Li_{1/4}FeF_3$ and $Li_{1/2}FeF_3$ (with average Fe oxidation states of 2.75+ and 2.5+, respectively) exist as stable phases upon reduction of $FeF_3$. These phases are derived from the rutile structure (see Figure 1 for TR $Li_{1/2}FeF_3$) by ordering Li and Fe on the metal site. Our NMR data do not provide any clear evidence for $Li_{1/4}FeF_3$ but do indicate that a phase with a composition close to $Li_{1/2}FeF_3$, with some of the structural features of rutile, does exist. Doe et al. proceeded to suggest that further lithiation can occur, particularly in the nanocomposites, to form the phases $Li_{1/2-x}Fe_{1+x}F_3$ (for example, $Li_{1/4}Fe_{5/4}F_3$ with an Fe oxidation state of 2.2+). The structures are derived from the TR structure, with Fe replacing Li in the metal sites of the structure to eventually form $FeF_2$. This can occur via the following reaction:

$$Li_{1/2}FeF_3 + \frac{3x}{2+2x}Li \rightarrow \frac{1}{1+x}Li_{1/2-x}Fe_{1+x}F_3 + \frac{3x}{1+x}LiF \quad (x \le 0.5) \quad (5)$$

So-called 1 × 1 tunnels are observed along the $c$ direction of the rutile and TR structures (Figure 1c,d), and a second mechanism analogous to that for rutile $TiO_2$ and nanoparticles of $\beta$-$MnO_2$, which have both been shown to accommodate Li by intercalation in their 1 × 1 tunnels,[30,31] is also possible:

$$Li_{1/2}FeF_3 + xLi \rightarrow Li_x[Li_{1/2}Fe]F_3 \quad (x \le 0.5) \quad (6)$$

The distance between the Fe atoms that form the tunnels in the TR structure (4.75 Å) is even larger than the Ti−Ti distance of rutile (4.59 Å), indicating that eq 6 is feasible. Clearly, the $ReO_3$ structure also has considerable empty space into which $Li^+$ can be inserted. Neither the LiF extrusion nor Li insertion mechanism involves the precipitation of Fe, consistent with the voltage profile until Li = 0.75. Distinct from the insertion mechanism(s), the LiF extrusion mechanism proposed by Doe et al.[10] involves the diffusion of Fe ions into the material and the formation of LiF. Some LiF is observed by XRD, consistent with either eq 4 or 5; however, the LiF concentration is not large, as it was not clearly observed using $^{19}$F in this range. It is also possible that the process shown in eq 6 occurs during the electrochemical reaction (because it may be kinetically favored) but that the lithiated phase can then react while the battery relaxes, precipitating out LiF and forming the products given by eqs 4

(30) Wagemaker, M.; Kearley, G. J.; van Well, A. A.; Mutka, H.; Mulder, F. M. *J. Am. Chem. Soc.* **2003**, *125*, 840–848.
(31) Armstrong, A. R.; Armstrong, G.; Canales, J.; Garcia, R.; Bruce, P. G. *Adv. Mater.* **2005**, *17*, 862–865.

and 5. The electrochemical profiles suggest that different mechanisms operate (or dominate) between Li = 0.5 and 0.75 and between Li = 0.75 and 1.0. The NMR resonances shift in the former range but remain constant in the latter. This fact, together with the noticeable drop in potential, may indicate that some $Fe^0$ has already started to form after Li = 0.75.

Reflections from LiF and Fe along with a number of unindexed peaks are observed in the second region (i.e., Li = 1.0 to 3.0). The $^{6,7}$Li and $^{19}$F NMR signals broaden noticeably, also indicating the formation of superparamagnetic particles of α-Fe. The resonance due to the insertion phase shifts on going from Li = 1.0 to 1.7 and decreases in intensity, essentially disappearing at Li = 3.0, indicating that the $Li_xFeF_3$ phase decomposes in this range. However, the shift of the Li NMR resonance indicates that this decomposition process involves intermediate phase(s), with a lower Fe oxidation state (presumably close to 2+). Furthermore, this confirms that even at Li = 1.0, the average Fe oxidation state of the $Li_xFeF_3$ intercalation phase must be still above 2+, consistent with the suggestion that some $Fe^0$ formation starts to occur for Li > 0.75.

The presence of sharp LiF reflections in the Li1.7 sample, which are not present for the Li3.0 sample, and the lack of significant reflections due to α-Fe are quite striking. These LiF reflections may arise from LiF formed during a reaction of the form given in eqs 4 and 5, while the conversion reaction involving the $Li_{1/2-x}Fe_{1+x}F_3$ phase results in much smaller (and/or disordered) LiF and α-Fe particles, so only broad XRD reflections are observed for these phases. The PDF data suggests that a rutile-like phase is still present in this range, while other broad reflections are also observed, indicating that an unidentified iron fluoride phase (perhaps an $Fe^{2+}$-doped LiF-derived phase or possibly the inverse spinel phase $Li_{3/2}Fe_{3/4}F_3$ proposed by Doe et al.[10]) may be present as well.

**Reaction Mechanism on Charge.** During the CCN-$FeF_3$ charge process, the steady decrease in the intensities of the XRD reflections due to α-Fe indicates that the conversion reaction is reversible. The particle sizes of the reconverted products must be small because their reflections are extremely broad, preventing identification of the products. However, a series of weak reflections are observed in the fully charged sample (C_Li0.5) at positions similar to those of the discharged Li0.5 sample. The observation that the $^6$Li resonances in the charged samples shift from 80 ppm for Li = 2.0 to ~168 ppm for Li = 0.5 indicates that the conversion products contain Li and that the reaction involves the removal of Li from the LiF/Fe nanocomposite to form a lithiated iron fluoride. The similar shifts of the fully charged sample and the Li0.5 sample formed on discharge indicate that the Li environments and Fe oxidation states are similar at this state of charge. This suggests that the material contains rutile-like structural features that are re-formed on charge, consistent with the PDF pattern of this material. This is in agreement with the work of Badway et al.,[24] who used electron diffraction and XRD to demonstrate that rutile was formed on charge. However, our NMR results demonstrate that in agreement with the mechanism proposed by Doe et al.,[10] the rutile phase formed on charge to potentials below 4.0 V is lithiated. Thus, for charge to 4.0 V, only 2.5 lithium atoms per Fe can be extracted from the material, and the charge process can be described as follows:

$$Fe + 3LiF \rightarrow \frac{1}{1+x}Li_{1/2-x}Fe_{1+x}F_3 + \frac{3x}{1+x}LiF \qquad (7)$$

Badway et al. have shown that additional Li can be removed above 4.0 V,[24] with the Li being removed from $Li_{1/2-x}Fe_{1+x}F_3$ to form the rutile phase $FeF_3$ (i.e., $Fe_{3/2}F_2$),[10] which presumably occurs at a higher potential since rutile is not the thermodynamic phase.

**Comparison with $FeF_2$.** The Li NMR spectra and XRD patterns clearly show that the reaction with $FeF_2$ involves both insertion and conversion reactions. The former cannot occur via a simple insertion of Li into the 1 × 1 tunnels of the structure for stoichiometric $FeF_2$, since $Fe^{2+}$ reduction to $Fe^+$ is not likely. Furthermore, on the basis of the hyperfine shifts seen in the $^6$Li NMR spectra of discharged CCN-$FeF_3$, the broad peak at 172−87 ppm observed for CCN-$FeF_2$ (Li = 0.25−0.5) corresponds to Li located near Fe with an average oxidation state between 2.5+ and 2+. Most of the Li insertion (~0.25 Li per Fe) appears to occur during a higher-potential window of 3.0−2.0 V (Figure 3b). The noticeable drop and then recovery of the potential occurring before the onset of the plateau at ~1.8 V, which is often associated with the nucleation of a new phase, may indicate the onset of the conversion reaction. Part of the insertion reaction may result from the reduction of $Fe^{3+}$ impurities present in the original starting material (present along with cation vacancies in a slightly defective rutile $Fe^{2+}{}_{1-3x}Fe^{3+}{}_{2x}F_2$) to form $Li_{2x}Fe_{1-x}F_2$, consistent with the potential seen for this process. These $Fe^{3+}$ impurities may arise from the ball-milling process, which was performed in air. There may also be oxide ion impurities. The reaction to form $Li_{2x}Fe_{1-x}F_2$, as written, must involve insertion of Li into both the rutile tunnels and cation vacancy sites, since there are insufficient cation vacancies to accommodate Li. The observation of LiF in the XRD pattern of the Li0.25 sample suggests that this process is associated with some LiF extrusion, presumably driven by the repulsions between cations in the tunnels and framework sites:

$$Li_{2x}Fe_{1-x}F_2 \rightarrow 2yLiF + Li_{2x-2y}Fe_{1-x}F_{2-2y} \qquad (8)$$

where $Li_{2x-2y}Fe_{1-x}F_{2-2y}$ corresponds to the rutile $Li_{2(x-y)/(1-y)}Fe_{(1-x)/(1-y)}F_2$. This reaction involves the nucleation and growth of only one new phase, LiF, as opposed to the final conversion reaction to form LiF and Fe, which involves the nucleation and growth of two separate phases.[32] We suggest that this accounts for the larger particles of LiF seen by XRD at this point. A similar explanation accounts for the larger LiF particles seen in the early stages of the $FeF_3$ lithiation. Again, the formation of LiF may represent a slower process that occurred as the samples were allowed to rest before the ex situ XRD measurements. Finally, we cannot exclude that an electrochemically driven disproportionation reaction mechanism involving formation of $Fe^0$ and $Fe^{3+}$ followed by reduction of $Fe^{3+}$ along with Li insertion accounts for some of the capacity. This process is likely to occur simultaneously, with Li insertion driving the extrusion of Fe out of the $FeF_2$ structure. This two-step mechanism can be written formally as follows:

$$FeF_2 \rightarrow Fe_{1-x}F_2(\text{rutile-type}) + xFe \qquad (9)$$

$$Fe_{1-x}F_2 + xLi \rightarrow Li_xFe_{1-x}F_2 \qquad (10)$$

Again, further Li insertion into the rutile tunnels to form $Li_x[Li_xFe_{1-x}]F_2$ is also possible. These reactions compete with the simple conversion reaction

(32) Yamakawa, N.; Jiang, M.; Grey, C. P. *Chem. Mater.* **2009**, in press.

$$FeF_2 + Li \rightarrow LiF + Fe \quad (11)$$

At the beginning of discharge, the Li insertion/extrusion reaction is favored over the conversion reaction, as indicated by the relative intensities of the Li resonances at ~172 and 0 ppm for the Li0.25 sample. As the discharge process proceeds, however, more and more $FeF_2$ is involved in the direct-conversion reaction, and the insertion phase decomposes to form LiF and Fe, resulting in a decrease in intensity of the 172 ppm peak for the Li0.5 sample.

## Conclusions

The reaction mechanisms of CCN-$FeF_3$ during both charge and discharge have been investigated using a combination solid-state NMR, XRD, and PDF methods. In particular, NMR and PDF studies are sensitive to local structural changes that occur in these poorly crystalline materials. The results provide strong evidence for the structural transformation of the $FeF_3$ phase from a $ReO_3$ structure to a phase that at least locally contains structural features resembling those of a lithiated rutile structure with an Fe oxidation state of close to 2.5+ and a composition close to $Li_{0.5}FeF_3$ on the first discharge, as suggested by Doe et al.[10] This material can accommodate more lithium by reducing the Fe to $Fe^{2+}$ and extruding LiF from the matrix. Some intercalation of Li into the tunnels or voids of this phase is also possible. The lithiated phase then decomposes to form nanoparticles of LiF and α-Fe, along with an as-yet-unidentified lithium iron fluoride phase. Surprisingly, we were able to obtain NMR spectra in this region, and they show that the α-Fe is superparamagnetic, consistent with the particle sizes obtained from diffraction. Both the NMR and PDF data indicate that the reconversion reaction occurs directly via the re-formation of a lithiated rutile phase, with the lithium incorporation and iron oxidation state increasing with state of charge. It should be noted that the increase in lithium content in the iron fluoride phase on charge is not intuitive but reflects the mechanism by which these phases convert from the Fe/LiF nanocomposite to the intercalation compound. The final material obtained on charge to 4.0 V, at least in our room-temperature studies, has a composition close to $Li_{0.5}FeF_3$, consistent with the capacity estimated from the electrochemical curve. The results were compared with those for rutile $FeF_2$, which was also lithiated on reduction, giving rise to resonances at shifts close to those seen in the $FeF_3$ system, indicating that the Li local environments are similar.

Although binary transition-metal compounds represent one of the more promising next-generation electrode materials and have much higher capacities than many electrode materials currently in use, the present work both highlights the complexity of the reactions that occur in these systems, which involve the formation of nanosized particles via a series of intermediate phases, and suggests characterization approaches that can be used to investigate these compounds. It is hoped that additional fundamental studies of the type reported here will provide the insights that are required in order to enhance the reversibility and rate performance of this class of materials, leading to improved control over the different reactions and phase transformations that occur in this and related systems.

**Acknowledgment.** This work was partially supported by the Assistant Secretary for Energy Efficiency and Renewable Energy, Office of FreedomCAR and Vehicle Technologies of the U.S. Department of Energy (DOE) under Contract DE-AC03-76SF00098 via Subcontract 6517749 with the Lawrence Berkeley National Laboratory, and by Sony Corporation. Use of the APS was supported by the U.S. DOE, Office of Science, Office of Basic Energy Sciences (BES), under Contract W-31-109-Eng-38. Use of the NSLS was supported by the U.S. DOE, BES (DE-AC02-98CH10886). We thank Peter Chupas, Evan Maxey, Jun Wang, Peter Stephens, and Kevin Stone for their help with data collection and analysis at the APS and NSLS. We thank Glenn Amatucci, Robert Doe, and Gerbrand Ceder for helpful discussions and sharing their paper (R.D., G.C.) with us before publication.

**Supporting Information Available:** Comparison of the refinement using PDF data for the Li0.5 sample with those for the $FeF_3$ and TR structures as structural models; evolution of the lattice parameters $a$ and $c$ derived using a TR model for Li = 0.5−1.0; and intensities derived from $^7$Li spin−echo experiments as a function of the spin evolution time, $\tau$, that were used to extract $T_2$ values. This material is available free of charge via the Internet at http://pubs.acs.org.

JA902639W